Oligocene deformation of the Chuandian terrane in the SE margin of the Tibetan Plateau related to the extrusion of Indochina

Journal Item

Tectonics

RESEARCH ARTICLE
10.1029/2019TC005974

Key Points:
- We revised the Lühe Basin sedimentation from late Miocene to 35–26.5 Ma by magnetostratigraphy and $^{40}Ar/^{39}Ar$ chronology
- Oligocene uplift of the SE Tibet margin is related to the extrusion and clockwise rotation of Indochina
- A reassessment on the age of other late Cenozoic basins in SE Tibet margin is required

Supporting Information:
- Supporting Information S1

Correspondence to:
S. Li,
s.li31@lancaster.ac.uk

Citation:
Li, S., Su, T., Spicer, R. A., Xu, C., Sherlock, S., Halton, A., et al. (2020). Oligocene deformation of the Chuandian terrane in the SE margin of the Tibetan Plateau related to the extrusion of Indochina. *Tectonics*, *39*, e2019TC005974. https://doi.org/10.1029/2019TC005974

Received 7 NOV 2019
Accepted 18 MAY 2020
Accepted article online 21 MAY 2020

Oligocene Deformation of the Chuandian Terrane in the SE Margin of the Tibetan Plateau Related to the Extrusion of Indochina

Shihu Li[1,2], Tao Su[3], Robert A. Spicer[3,4], Congli Xu[3], Sarah Sherlock[5], Alison Halton[5], Gregory Hoke[6], Yimin Tian[7], Shitao Zhang[7], Zhekun Zhou[3], Chenglong Deng[1,8,9], and Rixiang Zhu[1,8,9]

[1]State Key Laboratory of Lithospheric Evolution, Institute of Geology and Geophysics, Chinese Academy of Sciences, Beijing, China, [2]Lancaster Environment Centre, Lancaster University, Lancaster, UK, [3]CAS Key Laboratory of Tropical Forest Ecology, Xishuangbanna Tropical Botanical Garden, Chinese Academy of Sciences, Mengla, China, [4]School of Environment, Earth and Ecosystem Sciences, The Open University, Milton Keynes, UK, [5]School of Physical Sciences, The Open University, Milton Keynes, UK, [6]Department of Earth Sciences, Syracuse University, Syracuse, NY, USA, [7]Faculty of Land Resource Engineering, Kunming University of Science and Technology, Kunming, China, [8]Institutions of Earth Science, Chinese Academy of Sciences, Beijing, China, [9]College of Earth and Planetary Sciences, University of Chinese Academy of Sciences, Beijing, China

Abstract Mechanisms driving the tectonic evolution of the southeast (SE) margin of Tibet include the Paleogene extrusion of the coherent Indochina lithospheric block and the continuous deformation caused by lower crustal flow since the middle Miocene. The timing and style of regional deformations are keys to determining the role of each mechanism. Fault-bounded and fault-controlled Cenozoic basins within the SE margin of Tibet record regional deformation, surface uplift, and variations in paleoclimate but often are poorly dated. New magnetostratigraphy and $^{40}Ar/^{39}Ar$ dating of volcanic ashes constrain precisely the timing of sedimentation within the Lühe Basin to between ~35 and 26.5 Ma. The basin is located in the Chuandian terrane along the Chuxiong fault, which lies ~70 km north of, and parallel to, the Ailao Shan-Red River fault. The asymmetric syncline of the Lühe Basin suggests syncontractional sedimentation, and the basal age of the basin represents the initiation of the Chuxiong fault and crustal shortening at ~35 Ma. This is coincident with the onset of the Ailao Shan-Red River fault and supports a kinematic link between them. Our study suggests that, like the Ailao Shan-Red River fault, the Chuxiong fault is a Paleogene transpressional structure that developed during the extrusion and clockwise rotation of Indochina around the Eastern Himalayan Syntaxis, which caused the late Paleogene deformation and surface uplift of the Chuandian terrane and Indochina. Our revised chronostratigraphy of the Lühe Basin provides further evidence that many of the "Neogene" sedimentary basins in the SE margin of Tibet may be much older than previously thought.

1. Introduction

The temporal and spatial evolution of high topography in the Tibetan region during the India-Asia collision is key to understanding the geodynamics of intracontinental deformation as well as the link between plateau formation and global climate change. However, a critical element in understanding orogenic processes is the accurate dating of events. As one of the most important accommodation zones during the India-Asia collision, the tectonic deformation of the southeast (SE) margin of the Tibetan Plateau provides meaningful constraints on the tectonic evolution of the Tibetan Plateau. With the presence of several strike-slip faults thousands of kilometers long, for example, the Ailao Shan-Red River fault, an extrusion model was proposed, which suggested that the Asia portion of the huge India-Asia convergence was mainly accommodated in the SE margin of the Tibetan Plateau by early Cenozoic lateral extrusion of the largely coherent Indochina lithospheric block (Leloup et al., 1995; Tapponnier et al., 1982). However, based on the lack of significant upper crustal shortening in the SE margin of the Tibetan Plateau after the middle Miocene, some researchers proposed a lower crustal flow model. This envisages that ductile flow of the Tibetan lower crust into the margin of the SE Tibetan Plateau played a dominant role in accommodating the convergence between India and Asia after the middle Miocene (Clark and Royden, 2000; Royden et al., 1997). This lower crustal flow has

been invoked to produce the low-relief, high elevation topography in the SE margin of the Tibetan Plateau (Clark et al., 2006), although the origin of this low-relief remains controversial (Clark et al., 2006; Liu-Zeng et al., 2008; Yang et al., 2015). A compromise model is that the deformation in the SE margin of the Tibetan Plateau was dominated by lateral extrusion of Indochina in the early Cenozoic and by lower crustal flow since the middle Miocene (Schoenbohm et al., 2006). Precisely determining the timing of upper crustal deformation in the region is key to constraining the geodynamics on the evolution of the SE margin of the Tibetan Plateau, as well as large parts of the Tibetan region as a whole.

The surface uplift history of the SE margin of the Tibetan Plateau, despite decades of research, remains a controversial issue (e.g., Clark et al., 2005; Liu-Zeng et al., 2018; H. Zhang et al., 2016). Rapid incision of river gorges starting at ~15–10 Ma, documented by low-temperature thermochronology, serves as indirect evidence of surface uplift and river capture in the SE margin of the Tibetan Plateau, supposedly due to lower crustal flow (e.g., Clark et al., 2005; Ouimet et al., 2010). However, apart from the possible time lag between strong tectonic uplift and adjustment of drainage networks (e.g., Craddock et al., 2010), rapid river incision since the middle Miocene may also be the result of monsoon enhancement during the Middle Miocene Climate Optimum (Nie et al., 2018) and so cannot be used as a reliable proxy to date the inception of regional topographic rise. Furthermore, as a means of identifying the onset of surface uplift of the SE margin of the Tibetan Plateau, there has been a particular focus on constraining whether or not the Red River and Jinsha River were once connected (Clark et al., 2004). However, the timing of possible river captures, and subsequent drainage reorganization determined by provenance shifts, ranges from pre-Eocene to middle Miocene (e.g., Cao et al., 2018; Clift et al., 2006; Wissink et al., 2016; Yan et al., 2012). Recently, multiphased rapid uplift of the SE margin of the Tibetan Plateau, starting as early as the late Cretaceous, has been recognized by a growing number of low-temperature thermochronological studies (K. Cao et al., 2019; Liu-Zeng et al., 2018; Tian et al., 2014; Wang, Kirby, et al., 2012; Y. Wang et al., 2018) (Figure 1a).

Several stable isotope paleoaltimetry studies provide seemingly contradictory constraints on the surface elevation of the SE margin of the Tibetan Plateau (Gourbet et al., 2017; Hoke et al., 2014). Stable isotope paleoaltimetry of mountains and orogenic plateaus (e.g., Fan et al., 2017; Rowley & Garzione, 2007) relies heavily on appropriate assumptions of source water isotopic composition, air parcel trajectories, isotope elevation gradients, and paleoclimate, all of which are age dependent (Spicer et al., 2020). However, most of the Cenozoic basins in the SE margin of the Tibetan Plateau lack absolute age constraints, and the ages for these basins in the Chinese geologic maps have mainly relied on biostratigraphic and lithostratigraphic correlations. For example, the sedimentary rocks of the Jianchuan Basin were thought to have accumulated the most continuous sedimentary succession within the region, spanning the Paleocene to Pliocene (Yunnan Bureau of Geology and Mineral Resources Yunnan Bureau of Geology and Mineral Resource (YBGMR), 1990). Earlier paleoaltimetry studies from the Shuanghe Formation in the Jianchuan Basin assumed an early Miocene age and indicated that the basin had reached an elevation of ~2.6 km by that time (Hoke et al., 2014; Li, Currie, et al., 2015). However, a recent study by Gourbet et al. (2017) demonstrated that all the Oligocene to Pliocene rocks (Jinsichang, Shuanghe, and Jianchuan formations) are in fact late Eocene in age. Gourbet et al. (2017) applied a continentality effect correction and used a different initial $\delta^{18}O$ value to produce a revised paleoelevation of ~1.2 ± 1.2 km as a consequence. However, the validity of this correction was questioned by Wu et al. (2018), who suggested, based on stable isotope and pollen grain analyses, that a significant (but lower than today) elevation of 1.3–2.6 km was attained in the late Eocene. Within the eastern Qiangtang terrane, other radiometrically constrained paleoelevation estimates using plant fossils suggest that areas such as the Mangkang and Gonjo Basins were already at ~3 km by the end of the Eocene (Li, van Hinsbergen, et al., 2020; Su et al., 2019; Tang et al., 2017). Moreover, Hoke (2018) highlighted the northward decrease of 7.7‰ in the $\delta^{18}O$ of pedogenic carbonates from south to north across the SE margin of the Tibetan Plateau before any temperature corrections, which most likely suggests that a strong N-S gradient in elevation had already formed by the late Eocene. These paleoelevation disputes cannot be resolved unless the ages of the Cenozoic basins in the SE margin of the Tibetan Plateau are determined precisely.

The Lühe Basin, in the central part of the Yunnan Province of southwestern China (Figures 1 and 2), is another basin where previous studies have focused on paleoclimate (Xu et al., 2008), paleoelevation (Hoke et al., 2014; Li, Currie, et al., 2015), and river capture (Wissink et al., 2016). The age of the Lühe Basin was previously assigned to the late Miocene based on well-preserved plant fossils and regional

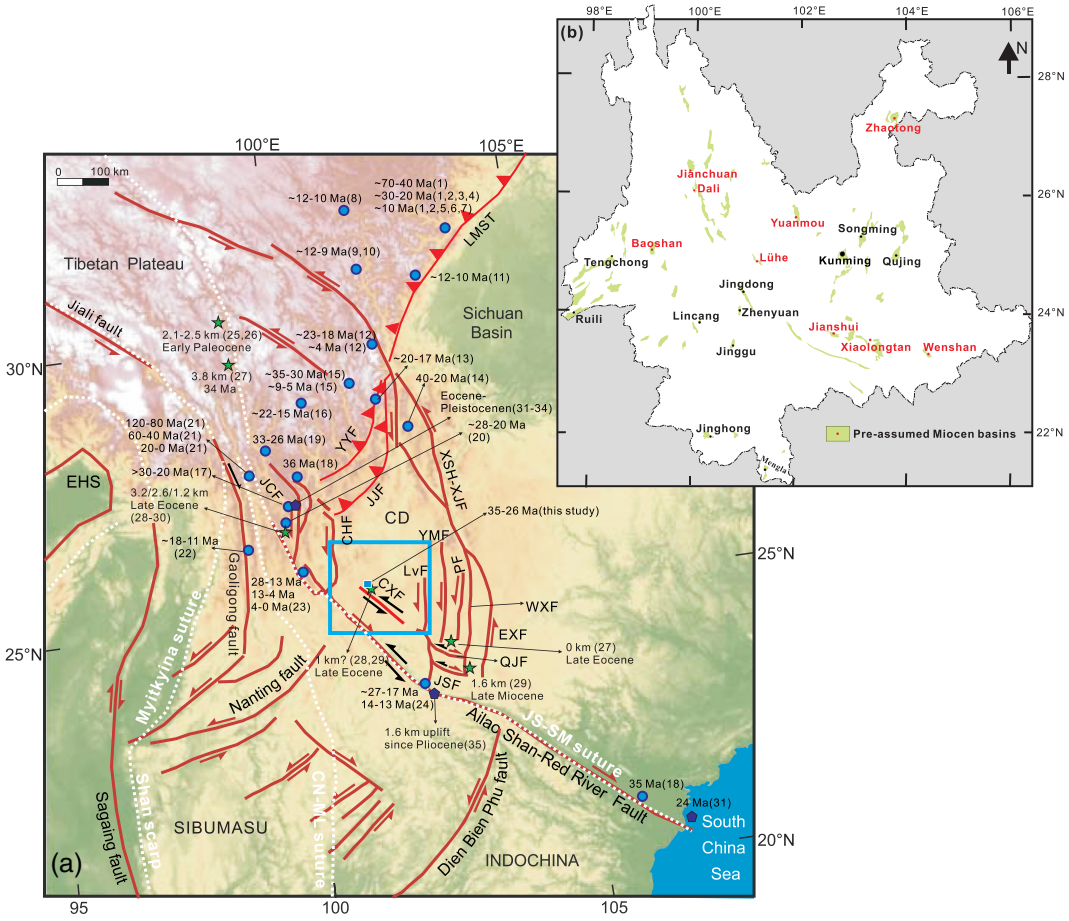

Figure 1. (a) Simplified geological map of the SE margin of the Tibetan Plateau, with major Cenozoic faults (black arrows represent the early Cenozoic faults; red arrows represent the late Miocene faults) and ages to constrain the uplift of the Tibetan Plateau SE margin. Blue dot: low-temperature thermochronology; green star: paleoelevation; purple polygon: river reorganization. Blue square represents the location of Figure 2. (b) Main sedimentary basins in Yunnan Province that were previously regarded in late Miocene based on biostratigraphy. The basins mentioned in the text are highlighted in red. CD: Chuandian terrane, CN-ML suture: Changning-Menglian suture, JS-SM suture: Jinshajiang-Song Ma suture, EHS: Eastern Himalaya Syntaxis, JCF: Jianchuan fault, CHF: Chenghai fault, CXF: Chuxiong fault, YYF: Yulong-Yunlong fault, JJF: Jinhe-Jianhe fault, LMST: Longmenshan thrust fault, XSH-XJF: Xianhuihe-Xiaojiang fault, LvF: Lvzhijiang fault, YMF: Yimenhe fault, PF: Puduhe fault, WXF: Western Xiaojiang fault, EXF: Eastern Xiaojiang fault, QJF: Qujiang fault, JSF: Jianshui fault. Reference: 1—Yang et al., 2017, 2—Wang, Kirby, et al., 2012, 3—Arne et al., 1997, 4—Wilson & Fowler, 2011, 5—Enkelmann et al., 2006, 7—Cook et al., 2013, 8—Tian et al., 2015; 9—Clark et al., 2005, 10—Ouimet et al., 2010, 11—Godard et al., 2009, 12—Xu & Kamp, 2000, 13—Wang, Jiang, et al., 2012, 14—Deng et al., 2017, 15—H. Zhang et al., 2016, 16—Tian et al., 2014, 17—Shen et al., 2016, 18—Lacassin et al., 1996, 19—Leloup et al., 2001, 20—K. Cao et al., 2019, 21—Liu—Zeng et al., 2018, 22—Y. Wang et al., 2018, 23—S. Y. Cao et al., 2011, 24—Y. Wang et al., 2016, 25—Tang et al., 2017, 26—Li, van Hinsbergen, et al., 2020, 27—Su et al., 2019, 28—Hoke et al., 2014, 29—Li, Currie, et al., 2015, 30—Gourbet et al., 2017, 31—Clift et al., 2006, 32—Yan et al., 2012, 33—Clark et al., 2004, 34—Kong et al., 2012, 35—Schoenbohm et al., 2004.

lithostratigraphic correlation (Wang, 1996; Yunnan Bureau of Geology and Mineral Resource (YBGMR), 1990). Using the Coexistence Approach, Xu et al. (2008) suggested that the Lühe area had a warm subtropical climate with more-than-present precipitation during the late Miocene. These paleoclimate proxy data were also used to reconstruct the paleoelevation of the Lühe area, which suggested an elevation of ~1 ± 0.8 km in the late Miocene (Hoke et al., 2014). However, Linnemann et al. (2018) reported a 33–32 Ma U-Pb zircon age of a primary volcanic ash within the plant-bearing sediments from the southern tip of the Lühe Basin (Lühe town section; see Figure 3 for location). This new age, together with updated ages from the Jianchuan Basin (Gourbet et al., 2017), is significantly transforming our view about the tectonics, paleoclimate, and biodiversity of the SE margin of the Tibetan Plateau (Hoke, 2018; Linnemann et al., 2018). But the number of well-dated successions remains woefully few. This initial glimpse is only the beginning, and additional radiometric and paleomagnetic age constraints of sedimentary basins throughout the SE margin of the Tibetan Plateau are essential for better understanding both the regional evolution and that of the Tibetan Plateau as a whole.

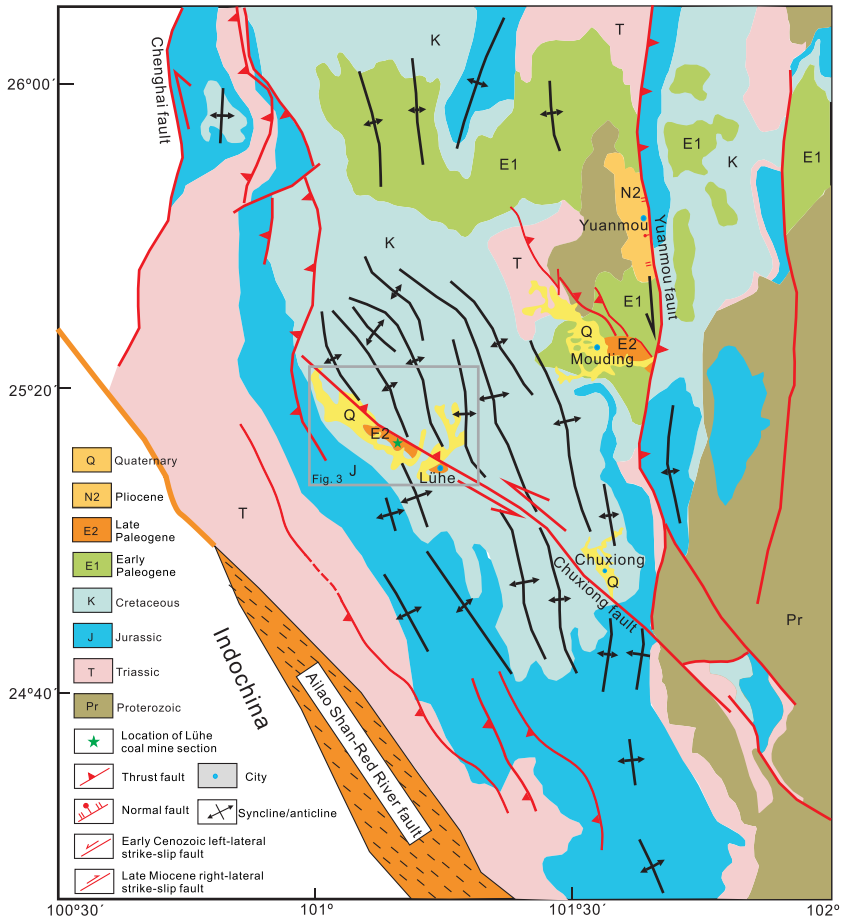

Figure 2. General geological map showing the structure relationships between the fold axes, thrust faults, and the Chuxiong fault in the Chuxiong Basin. Note that the fold axes are deflected when close to the Chuxiong fault, modified from Tapponnier et al. (1990). Green star and Lühe town denote the locations of our magnetostratigraphic section and Linnemann et al. (2018), respectively.

Here we combine magnetostratigraphy and $^{40}Ar/^{39}Ar$ dating of volcanic ashes exposed in the Lühe coal mine to constrain precisely the age of almost the entire sedimentary succession of the Lühe Basin. We also present structural evidence of regional folds and strike-slip faults, together with the geometry of the basin fill, to constrain the timing of tectonic processes that controlled the formation of the Lühe Basin. Finally, we reevaluate geodynamic models of tectonic deformation within the SE margin of the Tibetan Plateau by taking account of these new results.

2. Geological Setting

2.1. Regional Geological Background

The SE margin of the modern Tibetan Plateau refers to the fan-shaped area southeast of the Eastern Himalaya Syntaxis, between the Xianshuihe-Xiaojiang fault and the Shan scarp (Figure 1a). It comprises the Sibumasu and Indochina Blocks and the Chuandian terrane from west to east (Figure 1a). The Indochina Block is bounded to the west by the Changning-Menglian (CN-ML) suture zone, which separates it from the Sibumasu Block and to the east by the Jinshajiang-Song Ma suture, which separates it from the South China Block. The Chuandian terrane, a part of South China, is separated from the relatively stable South China Block by the Xianshuihe-Xiaojiang fault activated in the late Cenozoic due to the ongoing indentation of India with Asia. The northwestern boundary of the Chuandian terrane is uncertain but generally regarded as the Jinhe-Jianhe and the Yalong-Yulong thrust faults, the southwestern extension of the Longmen Shan thrust fault (Liu-Zeng et al., 2008; E. Wang et al., 1998).

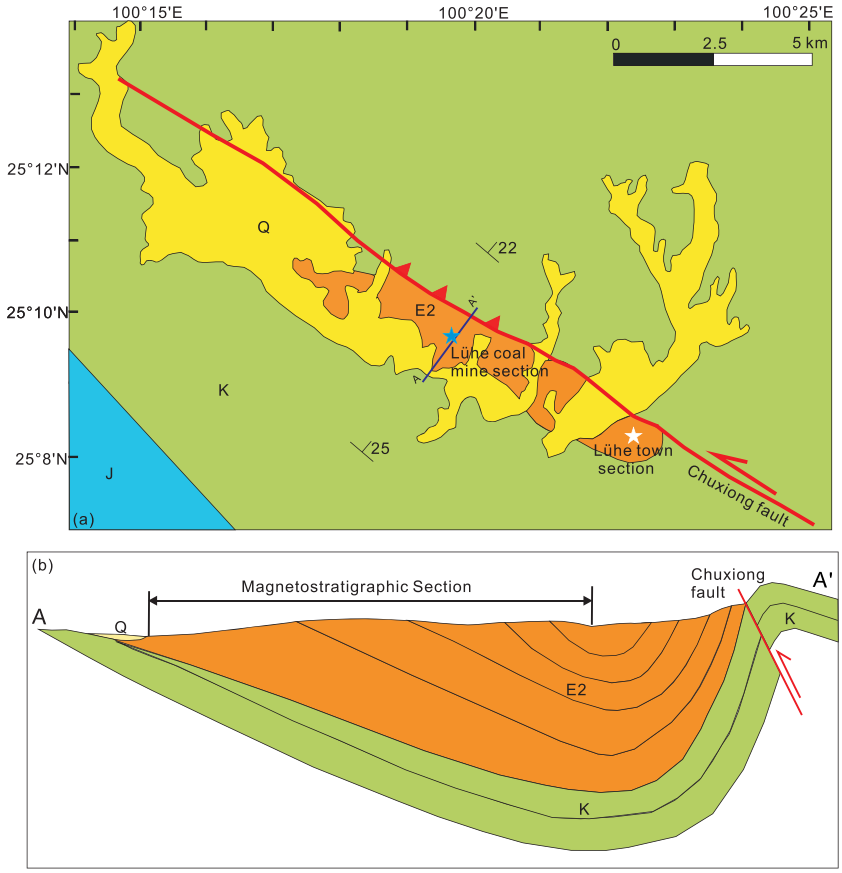

Figure 3. (a) Detailed geological map shows the structure relationship between the Chuxiong fault and Lühe Basin. (b) Cross section exhibits the syntectonic deposition of the Lühe Basin controlled by the Chuxiong fault. The abbreviations are the same as in Figure 2.

The SE margin of the Tibetan Plateau has experienced strong deformation since the late Cretaceous, which has resulted in a series of regional strike-slip faults (Leloup et al., 1995; E. Wang et al., 1998), tightly folded synclines and anticlines of Mesozoic-Cenozoic redbeds (Yunnan Bureau of Geology and Mineral Resource (YBGMR), 1990; Burchfiel & Chen, 2012), and a complex of regional high elevation and low-relief relict surfaces that are deeply dissected by continental scale rivers (Clark et al., 2006; Liu-Zeng et al., 2008).

The left-lateral Xianshuihe-Xiaojiang fault is one of the most important faults in the SE margin of the Tibetan Plateau and separates the strongly deformed Tibet from the relatively stable South China Block. It initiated at ~13 Ma (Li, Deng, et al., 2015; Roger et al., 1995; Y. Zhang et al., 2017) with a total offset about 80–100 km (E. Wang et al., 1998). The Ailao Shan-Red River fault is regarded as the eastern boundary of the Indochina extrusion and has experienced a major sinistral shear spanning 35–17 Ma (Leloup et al., 2001, 2007), with a hotly debated displacement of either 700 ± 200 or 250 km (see reviews in Leloup et al., 1995; Li et al., 2017; Searle et al., 2010, and references therein). Recent paleomagnetic reconstruction, however, showed that the displacement along the Ailao Shan-Red River fault is ~600 km in the northwest, but only 250 km in the southeast, which suggests that the Indochina Block did not behave as a rigid entity during the extrusion (Li et al., 2017). The motion on the Ailao Shan-Red River fault has reversed to act as a right-lateral fault since at least ~10 Ma with ~40 km displacement (Leloup et al., 1995; Li et al., 2013; Y. Wang et al., 2018), which was inferred to mark the onset of either the second stage of Tibet extrusion (Tapponnier et al., 1982) or lower crustal flow (Y. Wang et al., 2018).

Approximately 50–70 km north of the Ailao Shan-Red River fault, the Jianshui, Qujiang, and Chuxiong faults not only have a similar strike parallel to the Ailao Shan-Red River fault (Figure 1a) but also share a similar slip history to that of the Ailao Shan-Red River fault: an older left-lateral motion followed by

Figure 4. (a) Image shows the structure of the sediment packages exposed within the Lühe coal mine section. Red star denotes the location of volcanic ash for $^{40}Ar/^{39}Ar$ dating, yellow line represents the section for magnetostratigraphic study, and red line refers the unconformity of the Quaternary (Q) conglomerate on the Lühe Basin. (b) Picture shows the Cretaceous red beds thrust on the Lühe Basin. (c) Close-up view of the growth strata at the western limb of the syncline in the Lühe Basin. Note the truck in (a) and (b) and people in (c) for scales.

right-lateral reversal (Burchfiel & Wang, 2003; Leloup et al., 1995; Tapponnier et al., 1990; Figure 1a). These faults, together with the Ailao Shan-Red River fault, form a NW trending fault system in central Yunnan (Burchfiel & Wang, 2003). Although the offsets on these faults cannot be well constrained, all the pre-Pliocene rocks are left separated (Burchfiel & Wang, 2003; E. Wang et al., 1998), suggesting an early left-lateral slip. However, the active right-lateral displacement observed today is demonstrated by numerous Quaternary and Holocene geological features (Burchfiel & Wang, 2003; E. Wang et al., 1998), for example, scarps, deflected rivers, pull-apart basins, and seismic activity.

2.2. The Chuxiong Fault and Lühe Basin

The Chuxiong Basin is located between the Xianshuihe-Xiaojiang and Chenghai faults and north of the Ailao Shan-Red River fault (Figure 2). It is filled mainly by late Triassic-Paleocene red beds. Cenozoic basins are mainly developed along the strike-slip or thrust-faults and are regarded as late Miocene-Quaternary in age (Yunnan Bureau of Geology and Mineral Resource (YBGMR), 1990). The well-developed regional folds with NW-NNW trending axes in the Chuandian terrane (Figure 2) indicate NE-SW oriented shortening in the early Cenozoic (Leloup et al., 1995; Tapponnier et al., 1990; Yunnan Bureau of Geology and Mineral Resource (YBGMR), 1990). The Chuxiong fault is the main strike-slip fault in the Chuxiong Basin. As stated in section 2.1, it behaved as a left-lateral fault in the early Cenozoic, as evidenced by the bending of fold axes becoming more westerly trending as they approach the Chuxiong fault (Leloup et al., 1995; Tapponnier et al., 1990) (Figure 2). However, both the initial age and offset of the Chuxiong fault are poorly determined.

The Lühe Basin, a NWW-SEE trending narrow and elongated basin, is located on the southern side of the Chuxiong fault (Figure 3). The sedimentary rocks in the Lühe Basin are best exposed in the Lühe open pit coal mine, which are predominately marlstone, mudstone, sandstone, and coal (Figure 4). They rest unconformably on the Cretaceous red beds and are onlapped by Quaternary unconsolidated laterite (Figure 3). Numerous leaf, fruit, and seed fossils and palynoflora, such as *Tsuga* sp., *Calocedrus* sp., *Metasequoia* sp.,

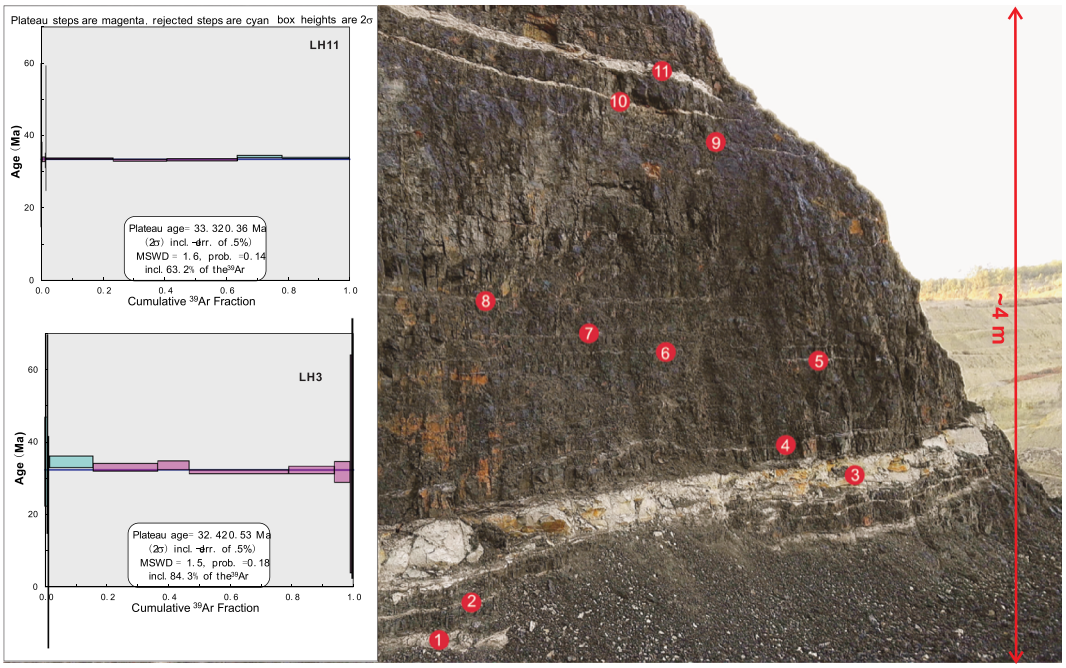

Figure 5. Detailed image shows the 11 volcanic ash layers observed within the coal beds at ~60 m of the Lühe coal mine section and the $^{40}Ar/^{39}Ar$ results of ash Layers 3 and 11.

Carpinus sp., *Alnus* sp., *Picea* sp., *Quercus* sp., are preserved in the Lühe Basin, which are similar to other late Miocene floras in Yunnan, and therefore, a late Miocene age was assigned to the Lühe Basin (Wang, 1996; Xu et al., 2008; Yunnan Bureau of Geology and Mineral Resource (YBGMR), 1990).

3. Methods

3.1. Sampling

The bottom of the Lühe coal mine (25.15°N/101.35°E) exposed an ~4 m thick stack of coal, within which 11 layers of volcanic ashes were recognized (Figure 5) ranging in thickness from >1 to ~30 cm. These ashes occur ~60 m from the base of the measured section (Figure 4a). Laser ablation $^{40}Ar/^{39}Ar$ dating of the thickest ash layers (3 and 11) constrains the age near the base of the measured section. The Lühe coal mine section where our paleomagnetic samples were collected has a total dip-corrected thickness of ~400 m along the easternmost side of the syncline (Figure 3a), but this depends on which part of the syncline was measured as the thickness of the rocks changes from the limb to the core. We did not observe any major unconformities, faults, or well-developed paleosols that may imply significant erosion or depositional hiatuses within the section. A total of 536 paleomagnetic samples was collected in the field with an interval of ~0.5 m (except the coal) using a gasoline powered drill. All samples were oriented in the field with a magnetic compass and were cut into one to two specimens (2.5 cm in diameter and 2.2 cm in height) in the laboratory.

3.2. $^{40}Ar/^{39}Ar$ Dating

Samples for $^{40}Ar/^{39}Ar$ dating were analyzed at the Open University, UK. The samples were crushed using a pestle and mortar, and the crushate was sieved and washed repeatedly in deionized water to remove dust and clay particles from the surfaces of all the size fractions. Sanidine, biotite, and feldspar crystals free from alteration were identified using a binocular microscope and hand-picked. The samples were cleaned ultrasonically in acetone and deionized water, dried using a hot plate, and packaged in aluminum foil packets of ~10 mm × 10 mm in size prior to irradiation.

Samples were irradiated at the McMaster Nuclear Reactor (McMaster University, Canada) for 100 hr. Cadmium shielding was used, and the samples were held in position 8D. Neutron flux was monitored using biotite mineral standard GA1550 which has an age of 99.738 ± 0.104 Ma (Renne et al., 2011). The

J values were then calculated by linear extrapolation between the two measured J values, and a 0.5% error on J was used.

Samples were analyzed using a Nu Instruments Noblesse and a 1,059 nm CSI fiber laser to melt/step heat the sample. Extracted gases were cleaned for 5 min using two SAES AP-10 getters running at 450°C and room temperature. System blanks were measured before every two sample analyses. Gas clean-up and inlet is fully automated, with measurement of ^{40}Ar, ^{39}Ar, ^{38}Ar, ^{37}Ar, and ^{36}Ar, each 10 scans, and the final measurements are extrapolations back to the inlet time.

Data reduction utilized in-house data reduction software, and all data were corrected for mass spectrometer discrimination using values of 305.2 for $^{40}Ar/^{36}Ar$, and system blanks were subtracted. Results were corrected for ^{37}Ar and ^{39}Ar decay since irradiation, and for neutron-induced interference reactions, using the following correction factors: $(^{39}Ar/^{37}Ar)_{Ca} = 0.00065 \pm 0.00000325$, $(^{36}Ar/^{37}Ar)_{Ca} = 0.000265 \pm 0.000001325$, and $(^{40}Ar/^{39}Ar)_{K} = 0.0085 \pm 0.0000425$ based on analyses of Ca and K salts. Ages were calculated using the atmospheric $^{40}Ar/^{36}Ar$ ratio of 298.56 (Lee et al., 2006) and decay constants of Renne et al. (2011). Isoplot V4.15 was used to calculate weighted averages and plateau ages, with all ages being reported at the 2σ level and including a 0.5% error on the J value. Plateau criteria of at least 50% of the ^{39}Ar release in at least three consecutive steps were used (see supporting information Table S1 for the full data).

3.3. Paleomagnetic Analysis

Similar to previous studies of the Xiaolongtan and Dali Basins (Li et al., 2013; Li, Deng, et al., 2015), the high organic content in the paleomagnetic samples from the Lühe Basin prevents an effective thermal demagnetization from being conducted; therefore, alternating field (AF) demagnetization was employed. All specimens were subjected to progressive AF demagnetization up to a maximum field of 60 mT, with 2.5–5 mT intervals below 30 mT and 10 mT intervals above 30 mT, using a 2G Enterprises Model 760 cryogenic magnetometer inside a magnetically shielded room (<300 nT). All the measurements were conducted in the Paleomagnetism and Geochronology Laboratory (PGL) in the Institute of Geology and Geophysics, Chinese Academy of Sciences.

The principal component analysis was computed either by least squares fit (Kirschvink, 1980) or by the great circle path (McFadden & McElhinny, 1988). The online tool set at Paleomagnetism.org (Koymans et al., 2016) was employed to analyze the data.

4. Results

4.1. Sedimentary Structures of the Lühe Basin

Like many of the other basins in Yunnan, the Lühe Basin was previously suggested to be an extensional basin along the dip-slip fault (e.g., Wang et al., 1998). However, the well-exposed section in the Lühe coal mine suggests that the Lühe Basin was deposited in a contractional setting (Figures 3 and 4). As shown in Figure 4b, the Chuxiong fault thrusts Cretaceous red beds over the Lühe Basin sedimentary rocks, forming a basin-scale plunging asymmetrical syncline. The thickness of strata in the eastern limb of the syncline is significantly greater than that of the western limb and increases away from the axis of the syncline (Figure 4a). The bedding dip of the eastern limb is much shallower than that of the western limb and increases toward the core of the syncline from ~20° to ~40°, while the bedding dips of the western limb decrease upward gradually from almost vertical to ~40° (Figure 4c). These lines of evidence suggest that the Lühe Basin is a syncontractional basin, and growth strata were deposited during the basin infill. The growth strata were further folded after basin infill was completed, forming the observed asymmetric syncline (Figure 4).

Thrust faults run parallel to the north and south of the Chuxiong fault and fold axes were also developed (Figure 2, Burchfiel & Wang, 2003). Leloup et al. (1995) noted that the Chuxiong fault obliquely traverses folds in the fold and thrust belt, and the folds bend into the fault on both sides. They interpreted the Chuxiong fault as a tear fault contemporaneous with the regional folding. Our field observations are consistent with the conclusion of Leloup et al. (1995) and Burchfiel and Wang (2003), suggesting that the Chuxiong fault is a left-lateral transpressional fault and the age of the Lühe Basin represents the onset of the Chuxiong fault movement and regional crustal shortening.

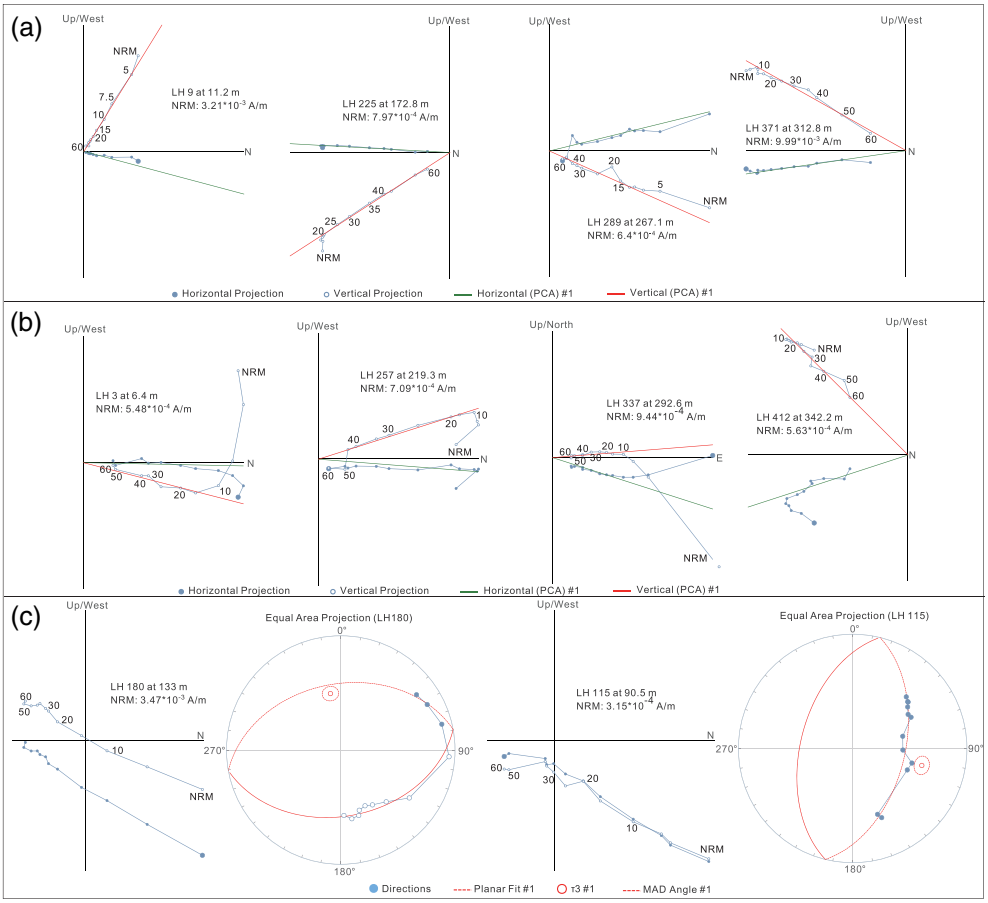

Figure 6. (a–c) Orthogonal vector plots of representative samples of progressive demagnetization. The solid (open) circles represent the horizontal (vertical) planes. NRM is the natural remanent magnetization.

4.2. $^{40}Ar/^{39}Ar$ Ages

The weighted average of 14 single grain fusion ages for biotites, from ash Horizon 3, ranged from 38.2 to 32.9 Ma with a weighted average of 36.09 ± 0.69 Ma, while step heating of a feldspar from the same horizon gave a younger age of 32.42 ± 0.53 Ma (Figure 5). The age discrepancy is possibly due to the heterogeneous incorporation of a minor component of excess ^{40}Ar which is not uncommon in volcanic biotites. We assume that the feldspar age most closely reflects the date of ash deposition and matches that of the youngest biotite. Step heating of a feldspar from ash Layer 11 gave a similar age of 33.32 ± 0.36 Ma, which is indistinguishable from that of ash Layer 3 when uncertainties are taken into account and suggests that the bottom part of the Lühe mine section was deposited at ~33 Ma, which is the same as U-Pb ages (33 ± 1 Ma) from zircons in primary ashes exposed ~2.6 km to the southeast in Lühe town (Linnemann et al., 2018; see Figure 3 for location).

4.3. Paleomagnetism

The demagnetization behavior of specimens from the Lühe mine section can be grouped into three types (Figure 6). The first type has only a single univectorial component decaying steadily toward the origin with an increasing field (Figure 6a). The demagnetization diagrams of the second type show two magnetic components (Figure 6b): a low-field magnetic component that was generally removed below 10 mT and above 10 mT a high-field magnetic component that decays linearly toward the origin and is regarded as the characteristic remanent magnetization (ChRM). The ChRMs of these two types were isolated between fields of 10 and 60 mT with at least four continuous demagnetization points. A few specimens show an overlap of two magnetic components, as suggested by the great circle paths on an equal-area diagram (Figure 6c). In this

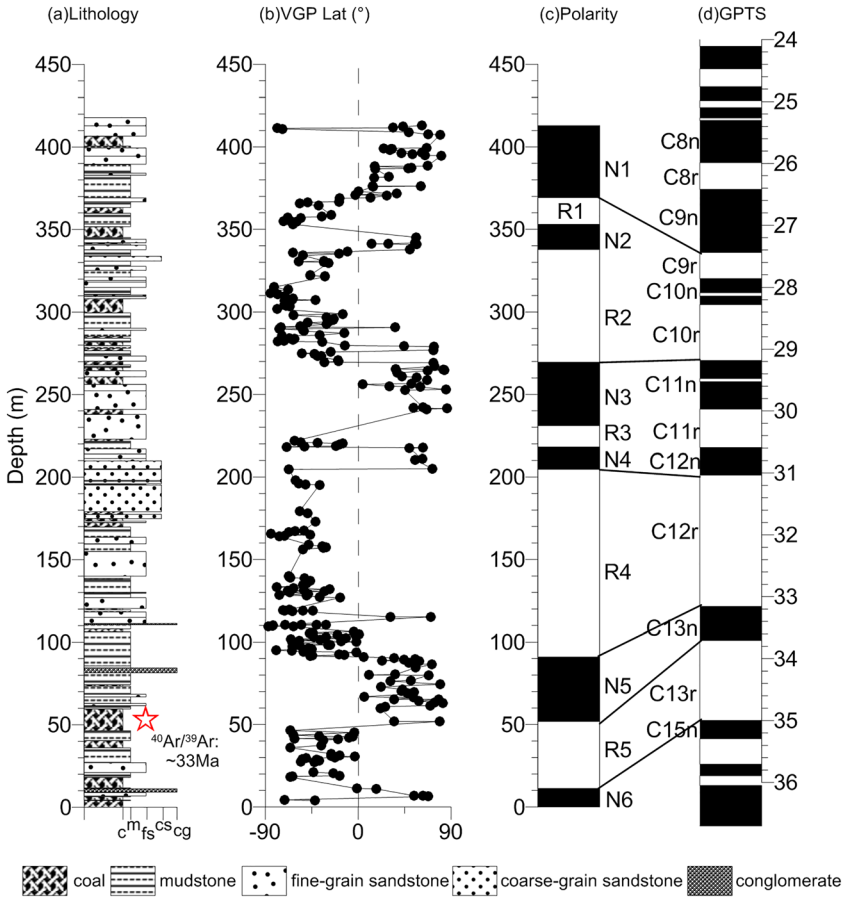

Figure 7. Lithology (a), virtual geomagnetic pole latitude (VGP Lat) (b), polarity (c) of the Lühe Basin and their correlation with the geomagnetic polarity timescale (GPTS) of Gradstein et al. (2012) (d). Red star denotes the location of volcanic ash in the section.

case, a great circle approach was used to approximate the ChRM direction based on the method of McFadden and McElhinny (1988). In total, 299 specimens yield interpretable ChRM directions used to construct the magnetic polarity stratigraphy.

4.4. Magnetostratigraphy

The ChRM directions were converted to virtual geomagnetic pole (VGP) latitudes to construct the magnetostratigraphy and correlate to the geomagnetic polarity time scale (GPTS, Gradstein et al., 2012). As shown in Figures 7, 11 magnetozones were identified in the studied section: 6 with normal polarity (N1–N6), while 5 exhibited reversed polarity (R1–R5). Each polarity zone was determined using at least four paleomagnetic sampling levels.

The ash layer at ~60 m in the section has a radiometric age of ~33 Ma, suggesting that the normal polarity zone N5 should be correlated to chron C13n. Based on this key age constraint, the studied section can be correlated well to chrons C15n–C9n of the GPTS, with an age span of ~35–26.5 Ma. Although our observed magnetozones can be straightforwardly correlated to the GPTS, we note that this correlation missed two short reversed polarities within chrons C11n and C10n, which may be caused by the low success rate in obtaining reliable paleomagnetic directions within the coals. Our magnetostratigraphic results therefore suggested that the age of the Lühe Basin is latest Eocene to late Oligocene (35–26.5 Ma) instead of late Miocene as previously assumed based solely on biostratigraphy.

5. Discussion

5.1. Implications for Ages of Other Late Cenozoic Basins in the SE Margin of the Tibetan Plateau

The SE margin of the Tibetan Plateau, especially in the Yunnan Province of southwestern China, hosts many sedimentary basins that contain abundant plant fossils and coal mines (Figure 1b). These basins provide an excellent archive of regional tectonics and so have been used frequently to constrain the reorganization of the regional drainage networks (e.g., Clark et al., 2004; Wissink et al., 2016), activation of regional strike-slip faults (Leloup et al., 1995; Li et al., 2013; E. Wang et al., 1998), climate change (Su et al., 2013; Xu et al., 2008), and paleoelevation reconstruction (Hoke et al., 2014; Li, Currie, et al., 2015; Wu et al., 2018). Yet the ages of most of these basins have not been well constrained and were generally regarded as Miocene or younger based largely on well-preserved plant fossils and interbasins correlations (Yunnan Bureau of Geology and Mineral Resource (YBGMR), 1990). Recent isotopic dating of the Jianchuan Basin (Gourbet et al., 2017; Hoke et al., 2014) and Lühe town section (Linnemann et al., 2018), however, both suggested Paleogene ages for sedimentary rocks that were previously assigned to the Miocene. Our new $^{40}Ar/^{39}Ar$ dating of volcanic ashes, together with a high-resolution magnetostratigraphy of the Lühe coal mine section, confirms the result of Linnemann et al. (2018) that the Lühe Basin was deposited in late Eocene-Oligocene time instead of the late Miocene as previously suggested. These new ages thus call for a reassessment of the ages of other late Cenozoic basins in the SE margin of the Tibetan Plateau, which were previously considered as late Miocene based solely on biostratigraphy. Moreover, magnetostratigraphic results, if based solely on plant fossils when correlating to the GPTS, should also be viewed with caution.

Magnetostratigraphic results from the Yuanmou, Xiaolongtan, Zhaotong, and Baoshan Basins (C. L. Deng et al., 2019; Ji et al., 2013; Li, Deng, et al., 2015; Li, Ji, et al., 2020; Zhu et al., 2005, 2008) are based not only on plant fossils but also on the biochronologically useful terrestrial faunas, including hominoid fossils, which are undoubtedly late Miocene in age (e.g., Harrison et al., 2002). Therefore, the late Miocene-Pliocene ages of these four basins, or at least parts of the sediment fills, constrained by magnetostratigraphy should still be reliable. A magnetostratigraphic study from the Wenshan Basin only identified two magnetozones and suggested a middle Miocene age based on plant fossils and regional stratigraphy correlation (Lebreton-Anberrée et al., 2016), and this age needs to be reassessed. The Dali Basin was regarded as late Miocene-Pleistocene based on a correlation of 26 magnetozones to GPTS constrained by the Sanying flora (Li et al., 2013), while a magnetostratigraphic study from the Jianshui Basin yielded a 4.8–1.7 Ma age based on an apparent correlation of 15 magnetozones to GPTS (Xiong et al., 2016). These dates may be more secure but ideally need to be corroborated using radiometric techniques.

The floras in basins of Tibetan Plateau SE margin, for example, Lühe, Xiaolongtan, Dali, and Wenshan, although ranging from Oligocene to Pliocene, are highly diverse, of modern appearance, and seem more or less unchanged through time (Linnemann et al., 2018). For example, there are 11 taxa cooccurring in both Lühe and Wenshan floras at genus level, 5 genera cooccurring in both the Lühe and Xiaolongtan floras, and 8 genera cooccurring in both the Sanying and Xiaolongtan floras (see supporting information Table S2 for detailed information). Therefore, it is difficult, if not impossible, to reliably use these plant fossils for age determination in other basins of the SE margin of the Tibetan Plateau or Yunnan, and so the validity of the middle Miocene age of the Wenshan Basin, the late Miocene-Pleistocene age of the Dali Basin, and the Pliocene-Pleistocene age of the Jianshui Basin needs to be further investigated by radiometric dating. Caution must be exercised when using the Miocene ages to estimate regional tectonics and climate change. Further discovery of radiometrically dateable tephras in the basins of the SE margin of the Tibetan Plateau is essential to advance our understanding of regional tectonics, orographic, climate, and biodiversity evolution.

5.2. Oligocene Deformation of the SE Margin of the Tibetan Plateau

Our magnetostratigraphic result suggests that the Lühe Basin developed from 35 to 26.5 Ma. The changing of bedding attitudes and thicknesses of strata in the Lühe coal mine section (Figure 4) suggests that the Lühe Basin is a syntectonic basin deposited in a compressional setting controlled by the Chuxiong fault, and asymmetrical growth strata were developed during the subsidence of the basin and subsequently folded (Figure 4). Therefore, the crustal shortening of the Chuandian terrane occurred synchronously with the onset of the Lühe Basin deposition at ~35 Ma and persisted after the cessation of deposition at ~26 Ma. A provenance study of fluvial sandstones from the Lühe coal mine section shows that the youngest and

most abundant zircon U-Pb peak of ~33–35 Ma (Wissink et al., 2016) is consistent with the age of volcanic ashes at the bottom of the section. Although the source of the volcanics was not constrained, the concordant age between the youngest detrital zircon and volcanic ashes may suggest the erosion of contemporaneous local sediments recycled into the basin or direct airfall zircon grains mixed with detrital grains in the sedimentary system.

Regionally, numerous studies applying different methods have been used to characterize the topographic history of the SE margin of the Tibetan Plateau. Since it remains unclear whether or not the paleo-Red River existed (e.g., Wei et al., 2016; Wissink et al., 2016; P. Zhang et al., 2019), the timing of uplift derived from river captures will not be considered here. Earlier low-temperature thermochronology studies suggested a middle-late Miocene (13–9 Ma, Serravallian-Tortonian) rapid rock uplift of the eastern and SE margin of the Tibetan Plateau (Clark et al., 2005; Kirby et al., 2002; Ouimet et al., 2010; Figure 1), but later studies revealed episodic rock uplift of the area prior to the late Miocene, especially in the Oligocene (K. Cao et al., 2019; Liu-Zeng et al., 2018; Tian et al., 2014; Wang, Kirby, et al., 2012; Y. Wang et al., 2018).

Paleoelevation reconstructions have indicated that the northwestern part (north of Dali) of the SE margin of the Tibetan Plateau had achieved near-present-day elevations by the latest middle Eocene (~40 Ma) (Hoke et al., 2014; Su et al., 2019). This result still stands, even if the presumed Miocene strata in the Jianchuan Basin, north of Dali, are actually Eocene in age (Gourbet et al., 2017). Of the three basins southeast of Dali, two, Lühe and Xiaolongtan, were assigned the late Miocene based on biostratigraphy, while the Chake Basin is the Eocene. However, this study and Linnemann et al. (2018) squarely assign the sediments of the Lühe Basin to the late Paleogene and paleoaltimetry results still imply that the area around Lühe was lower in the Eocene (Hoke et al., 2014; Li, Currie, et al., 2015). Notably, the rocks of Jinsichang, Shuanghe, and Jianchuan formations in the Jianchuan Basin, which are dominated by sandstones, conglomerates, and volcaniclastics and have a total thickness of at least more than 3 km (Yunnan Bureau of Geology and Mineral Resource (YBGMR), 1990), have been precisely dated as ranging from 37 to 34 Ma (Gourbet et al., 2017). This would suggest a high sediment accumulation rate during this interval and thus rapid uplift of mountains surrounding the Jianchuan Basin. In summary, the Oligocene crustal shortening of Chuandian terrane documented from the Lühe Basin is broadly coeval with other uplift events around the SE margin of the Tibetan Plateau (Figure 1), suggesting a regional elevation rise beginning before the Oligocene. Nevertheless, we should emphasize that this deformation does not mean that the near-present elevation of all the SE margin of the Tibetan Plateau was achieved in the Paleogene.

5.3. Geodynamics and Tectonic Evolution of the Tibetan Plateau

In the classical extrusion model, the Indochina Block is supposed to have behaved as a coherent lithospheric block during the early Cenozoic, undergoing eastward extrusion and clockwise rotation (Leloup et al., 1995; Tapponnier et al., 1982). If that was the case, we would not expect too much deformation within the Indochina Block. However, as observed by many previous studies, the tectonic deformation in the northwestern part of the block is significantly greater than that in the southeast (e.g., Hoke et al., 2014; Liu-Zeng et al., 2008). The well-developed strike-slip faults in the northwestern Indochina, such as the Nantinghe fault and Dien Bien Phu fault (e.g., E. Wang et al., 1998), and differential clockwise rotations within Indochina as suggested by numerous paleomagnetic studies (e.g., Li et al., 2017; Tong et al., 2013), further indicate that the block has deformed internally while remaining largely coherent. Based on a comprehensive review on all the available paleomagnetic data from the SE margin of the Tibetan Plateau and plate reconstructions, Li et al. (2017) proposed that the Indochina did not behave as a rigid block during extrusion and clockwise rotation but instead can be divided into four quasi-rigid subterranes with differential clockwise rotations (Li et al., 2017) (Figure 8). This nonrigid extrusion incorporates a north to south gradient in displacement along the Ailao Shan-Red River fault, with ~600 km in the northwest, while only 250 km was transferred to the southeast. This reconciles the long-term debates regarding the “small” and “large” displacement along the Ailao Shan-Red River fault. Moreover, the nonrigid extrusion of Indochina implies that a large portion (~350 km) of the extrusion was accommodated by internal crustal shortening (the gray areas in Figure 8) and differential clockwise rotation within the Indochina Block (Li et al., 2017), which permits significant surface uplift and the occurrence of strike-slip faults in the SE margin of the Tibetan Plateau during the early Cenozoic.

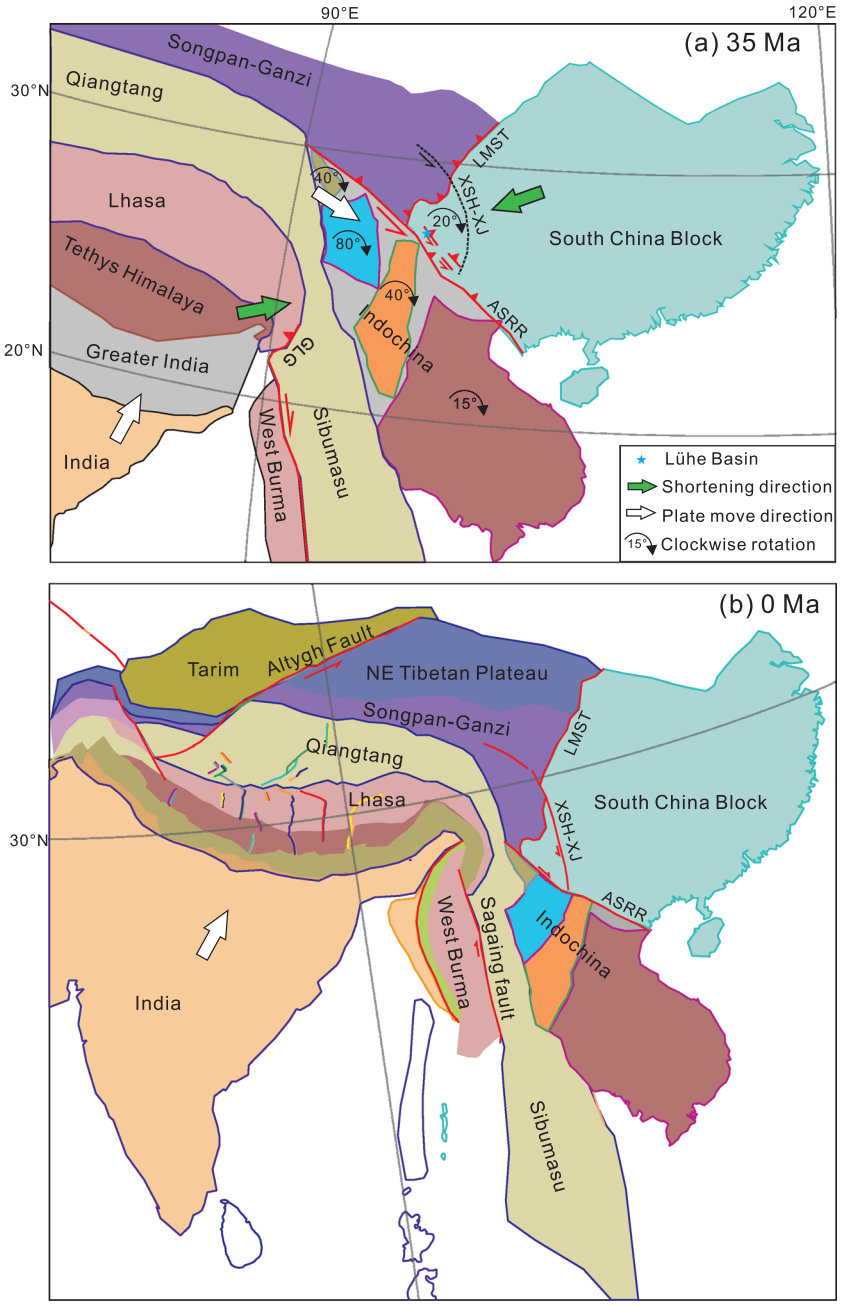

Figure 8. Schematic map showing the deformation in the SE margin of the Tibetan plateau at 35 Ma (a) and present (b) based on the reconstruction of Li et al. (2017), Liu-Zeng et al. (2018), and van Hinsbergen et al. (2019). The blue star represents the site of this study. Large arrows highlight the direction of compressional strain and clockwise rotation around the Eastern Himalaya Syntaxis. Dashed line represents the future Xianshuihe-Xiaojiang (XSH-XJ) fault at 15 Ma. The gray areas in the Indochina Block denote the amount of shortening during the Cenozoic extrusion and differential rotation of Indochina. ASRR: Ailao Shan-Red River fault, LMST: Longmen Shan Thrust fault, GLG: Gaoligong fault.

Our study from the Lühe Basin suggests that the Chuxiong fault experienced transpressive deformation with left-lateral movement as early as ~35 Ma, which is concurrent with the onset of sinistral shear on the Ailao Shan-Red River fault (Leloup et al., 2001, 2007). The crustal deformation of the Chuandian terrane started at 35 Ma is also consistent with previous low-temperature thermochronological results from other parts of the SE margin of the Tibetan Plateau that suggest an episode of rapid uplift in the Oligocene (H. Zhang et al., 2016; K. Cao et al., 2019; Liu-Zeng et al., 2018; Tian et al., 2014; Wang, Kirby, et al., 2012). The

strongly coupled time, slip sense, and fault geometry between the Ailao Shan-Red River and Chuxiong faults and the synchronous uplift of the SE margin of the Tibetan Plateau suggest that nonrigid extrusion and clockwise rotation of Indochina, beginning in the late Eocene-Oligocene, caused the surface uplift of the SE margin of the Tibetan Plateau at this time (Figure 8).

However, we are fully aware that evidence for uplift of the SE margin of the Tibetan Plateau in the Oligocene does not preclude the possibility that significant crustal thickening and uplift, and therefore, a high elevation in the SE margin of the Tibetan Plateau may have occurred prior to or after the Oligocene. As suggested by Liu-Zeng et al. (2018) and many others, the SE margin of the Tibetan Plateau may have experienced a multi-phased uplift, and a rapid rise could have started as early as the late Cretaceous or early Cenozoic (Li, van Hinsbergen, et al., 2020; Liu-Zeng et al., 2018), at the beginning of the India-Asia collision. A late Miocene uplift, as suggested by many low-temperature thermochronological studies, may have been associated with lower crustal flow (Clark et al., 2005), enhanced monsoon (Nie et al., 2018), base-level fall caused by fault related river captures (Hoke et al., 2014; Li, Currie, et al., 2015), or a combination thereof.

6. Conclusions

In this study we present high-resolution magnetostratigraphy and $^{40}Ar/^{39}Ar$ dating of the Lühe coal mine section within the Lühe Basin on the SE margin of the Tibetan Plateau, which constrains precisely the Lühe Basin fill, as exposed in the Lühe coal mine, accumulated from 35 to 26.5 Ma. This age is significantly older than the late Miocene, which was assigned previously based on plant fossils and lithostratigraphic correlation. This study therefore supports the suggestion of recent studies (e.g., Gourbet et al., 2017; Linnemann et al., 2018) that many supposedly Neogene sedimentary basins in Yunnan may be much older than previously thought and calls a careful reassessment of the age of other late Cenozoic basins in the SE margin of the Tibetan Plateau. Structures in the Lühe Basin and the surrounding region suggest that development of the Lühe Basin was controlled by the left-lateral transpressional Chuxiong fault, indicating that the Chuxiong fault and crustal shortening of the Chuandian terrane began at ~35 Ma. The synchronicity of activity along both the Chuxiong and Ailao Shan-Red River faults and crustal shortening of the Chuandian terrane together with other parts of the SE margin of the Tibetan Plateau indicate that the late Paleogene uplift of the SE margin of the plateau is most likely related to the nonrigid extrusion and clockwise rotation of Indochina at this time.

Data Availability Statement

The original paleomagnetic data of this paper can be accessed through the public domain repository Zenodo (https://doi.org/10.5281/zenodo.3525464).

Acknowledgments

We are grateful to the Associate Editor, Professor Majie Fan, and two reviewers, Professor P. H. Leloup and Professor Weitao Wang for their insightful comments and suggestions. We appreciate Huasheng Huang for his assistance during fieldwork. This study was funded by the National Natural Science Foundation of China (NSFC) Grants 41888101, 41690112, and 41772026. Shihu Li acknowledges the further support from the Royal Society-K.C.Wong International Fellowship. R. A. S. acknowledges support from NSFC-NERC (Natural Environment Research Council of the UK) joint research program (41661134049 and NE/P013805/1) and an XTBG International Fellowship for Visiting Scientists.

References

Arne, D., Worley, B., Wilson, C., Chen, S. F., Foster, D., Luo, Z. L., et al. (1997). Differential exhumation in response to episodic thrusting along the eastern margin of the Tibetan Plateau. *Tectonophysics*, *280*(3-4), 239–256. https://doi.org/10.1016/S0040-1951(97)00040-1

Burchfiel, B. C., & Chen, Z. (2012). Tectonics of the southeastern Tibetan Plateau and its adjacent foreland. *Geological Society of America Memoirs*, *210*, 1–165.

Burchfiel, B. C., & Wang, E. C. (2003). Northwest-trending, middle Cenozoic, left-lateral faults in southern Yunnan, China, and their tectonic significance. *Journal of Structural Geology*, *25*(5), 781–792. https://doi.org/10.1016/S0191-8141(02)00065-2

Cao, K., Wang, G., Leloup, P. H., Mahéo, G., Xu, Y., van der Beek, P. A., et al. (2019). Oligocene-Early Miocene topographic relief generation of southeastern Tibet triggered by thrusting. *Tectonics*, *38*, 374–391. https://doi.org/10.1029/2017TC004832

Cao, L., Shao, L., Qiao, P., Zhao, Z., & van Hinsbergen, D. J. J. (2018). Early Miocene birth of modern Pearl River recorded low-relief, high-elevation surface formation of SE Tibetan Plateau. *Earth and Planetary Science Letters*, *496*, 120–131. https://doi.org/10.1016/j.epsl.2018.05.039

Cao, S. Y., Neubauer, F., Liu, J. L., Censer, J., & Leiss, B. (2011). Exhumation of the Diancang Shan metamorphic complex along the Ailao Shan-Red River belt, southwestern Yunnan, China: Evidence from Ar-40/Ar-39 thermochronology. *Journal of Asian Earth Sciences*, *42*(3), 525–550. https://doi.org/10.1016/j.jseaes.2011.04.017

Clark, M., House, M. A., Royden, L. H., Whipple, K. X., Burchfiel, B. C., Zhang, X., & Tang, W. (2005). Late Cenozoic uplift of southeastern Tibet. *Geology*, *33*(6), 525–528. https://doi.org/10.1130/G21265.1

Clark, M., Royden, L., Whipple, K., Burchfiel, B., Zhang, X., & Tang, W. (2006). Use of a regional, relict landscape to measure vertical deformation of the eastern Tibetan Plateau. *Journal of Geophysical Research*, *111*, F03002. https://doi.org/10.1029/2005JF000294

Clark, M., & Royden, L. H. (2000). Topographic ooze: Building the eastern margin of Tibet by lower crustal flow. *Geology*, *28*(8), 703–706. https://doi.org/10.1130/0091-7613(2000)28<703:TOBTEM>2.0.CO;2

Clark, M., Schoenbohm, L. M., Royden, L. H., Whipple, K. X., Burchfiel, B. C., Zhang, X., et al. (2004). Surface uplift, tectonics, and erosion of eastern Tibet from large-scale drainage patterns. *Tectonics*, *23*, TC1006. https://doi.org/10.1029/2002TC001402

Clift, P., Blusztajn, J., & Duc, N. A. (2006). Large-scale drainage capture and surface uplift in eastern Tibet-SW China before 24 Ma inferred from sediments of the Hanoi Basin, Vietnam. *Geophysical Research Letters*, *33*, L19403. https://doi.org/10.1029/2006GL027772

Cook, K. L., Royden, L. H., Burchfiel, B. C., Lee, Y. H., & Tan, X. (2013). Constraints on Cenozoic tectonics in the southwestern Longmen Shan from low-temperature thermochronology. *Lithosphere*, *5*(4), 393–406. https://doi.org/10.1130/L263.1

Craddock, W. H., Kirby, E., Harkins, N. W., Zhang, H., Shi, X., & Liu, J. (2010). Rapid fluvial incision along the Yellow River during headward basin integration. *Nature Geoscience*, *3*(3), 209–213. https://doi.org/10.1038/ngeo777

Deng, B., Liu, S., Jiang, L., Zhao, G., Huang, R., Li, Z., et al. (2017). Tectonic uplift of the Xichang Basin (SE Tibetan Plateau) revealed by structural geology and thermochronology data. *Basin Research*, *30*(1), 75–96.

Deng, C. L., Hao, Q. Z., Guo, Z. T., & Zhu, R. X. (2019). Quaternary integrative stratigraphy and timescale of China. *Science China Earth Sciences*, *62*(1), 324–348. https://doi.org/10.1007/s11430-017-9195-4

Enkelmann, E., Ratschbacher, L., Jonckheere, R., Nestler, R., Fleischer, M., Gloaguen, R., et al. (2006). Cenozoic exhumation and deformation of northeastern Tibet and the Qinling: Is Tibetan lower crustal flow diverging around the Sichuan Basin? *Geological Society of America Bulletin*, *118*(5-6), 651–671. https://doi.org/10.1130/B25805.1

Fan, M., Constenius, K. N., & Dettman, D. L. (2017). Prolonged high relief in the northern Cordilleran orogenic front during middle and late Eocene extension based on stable isotope paleoaltimetry. *Earth and Planetary Science Letters*, *457*, 376–384. https://doi.org/10.1016/j.epsl.2016.10.038

Godard, V., Pik, R., Lavé, J., Cattin, R., Tibari, B., de Sigoyer, J., et al. (2009). Late Cenozoic evolution of the central Longmen Shan, eastern Tibet: Insight from (U-Th)/He thermochronometry. *Tectonics*, *28*, TC5009. https://doi.org/10.1029/2008TC002407

Gourbet, L., Leloup, P. H., Paquette, J.-L., Sorrel, P., Maheo, G., Wang, G., et al. (2017). Reappraisal of the Jianchuan Cenozoic basin stratigraphy and its implications on the SE Tibetan plateau evolution. *Tectonophysics*, *700-701*, 162–179. https://doi.org/10.1016/j.tecto.2017.02.007

Gradstein, F. M., Ogg, G., & Schmitz, M. (2012). *The geologic time scale 2012*. Oxford, UK: Elsevier.

Harrison, T., Ji, X. P., & Su, D. (2002). On the systematic status of the late Neogene hominoids from Yunnan Province, China. *Journal of Human Evolution*, *43*(2), 207–227. https://doi.org/10.1006/jhev.2002.0570

Hoke, G. D. (2018). Geochronology transforms our view of how Tibet's southeast margin evolved. *Geology*, *46*(1), 95–96. https://doi.org/10.1130/focus012018.1

Hoke, G. D., Liu-Zeng, J., Hren, M. T., Wissink, G. K., & Garzione, C. N. (2014). Stable isotopes reveal high southeast Tibetan Plateau margin since the Paleogene. *Earth and Planetary Science Letters*, *394*, 270–278. https://doi.org/10.1016/j.epsl.2014.03.007

Ji, X. P., Jablonski, N. G., Su, D. F., Deng, C. L., Flynn, L. J., You, Y., & Kelley, J. (2013). Juvenile hominoid cranium from the terminal Miocene of Yunnan, China. *Science Bulletin*, *58*(31), 3771–3779. https://doi.org/10.1007/s11434-013-6021-x

Kirby, E., Reiners, P. W., Krol, M. A., Whipple, K. X., Hodges, K. V., Farley, K. A., et al. (2002). Late Cenozoic evolution of the eastern margin of the Tibetan Plateau: Inferences from 40Ar/39Ar and (U-Th)/He thermochronology. *Tectonics*, *21*(1), TC1001. https://doi.org/10.1029/2000TC001246

Kirschvink, J. (1980). The least-squares line and plane and the analysis of palaeomagnetic data. *Geophysical Journal International*, *62*(3), 699–718. https://doi.org/10.1111/j.1365-246X.1980.tb02601.x

Kong, P., Zheng, Y., & Caffee, M. W. (2012). Provenance and time constraints on the formation of the first bend of the Yangtze River. *Geochemistry, Geophysics, Geosystems*, *13*, Q06017. https://doi.org/10.1029/2012GC004140

Koymans, M. R., Langereis, C. G., Pastor-Galán, D., & van Hinsbergen, D. J. J. (2016). Paleomagnetism.org: An online multi-platform open source environment for paleomagnetic data analysis. *Computers and Geosciences*, *93*, 127–137. https://doi.org/10.1016/j.cageo.2016.05.007

Lacassin, R., Scharer, U., Leloup, P. H., Arnaud, N., Tapponnier, P., Liu, X. H., & Zhang, L. S. (1996). Tertiary deformation and metamorphism SE of Tibet: The folded tiger-leap decollement of NW Yunnan, China. *Tectonics*, *15*(3), 605–622. https://doi.org/10.1029/95TC03749

Lebreton-Anberrée, J., Li, S., Li, S.-F., Spicer, R. A., Zhang, S.-T., Su, T., et al. (2016). Lake geochemistry reveals marked environmental change in Southwest China during the Mid Miocene Climatic Optimum. *Science Bulletin*, *61*(11), 897–910. https://doi.org/10.1007/s11434-016-1095-x

Lee, J.-Y., Marti, K., Severinghaus, J. P., Kawamura, K., Yoo, H.-S., Lee, J. B., & Kim, J. S. (2006). A redetermination of the isotopic abundances of atmospheric Ar. *Geochimica et Cosmochimica Acta*, *70*(17), 4507–4512. https://doi.org/10.1016/j.gca.2006.06.1563

Leloup, P., Lacassin, R., Tapponnier, P., Scharer, U., Zhong, D. L., Liu, X. H., et al. (1995). The Ailao Shan-Red River shear zone (Yunnan, China), Tertiary transform boundary of Indochina. *Tectonophysics*, *251*(1-4), 3–84. https://doi.org/10.1016/0040-1951(95)00070-4

Leloup, P. H., Arnaud, N., Lacassin, R., Kienast, J. R., Harrison, T. M., Trong, T. T. P., et al. (2001). New constraints on the structure, thermochronology, and timing of the Ailao Shan-Red River shear zone, SE Asia. *Journal of Geophysical Research*, *106*(B4), 6683–6732. https://doi.org/10.1029/2000JB900322

Leloup, P. H., Tapponnier, P., Lacassin, R., & Searle, M. P. (2007). Discussion on the role of the Red River shear zone, Yunnan and Vietnam, in the continental extrusion of SE Asia. *Journal of the Geological Society*, *164*(6), 1253–1260. https://doi.org/10.1144/0016-76492007-065

Li, S. H., Advokaat, E. L., van Hinsbergen, D. J. J., Koymans, M., Deng, C., & Zhu, R. (2017). Paleomagnetic constraints on the Mesozoic-Cenozoic paleolatitudinal and rotational history of Indochina and South China: Review and updated kinematic reconstruction. *Earth-Science Reviews*, *171*, 58–77. https://doi.org/10.1016/j.earscirev.2017.05.007

Li, S. H., Deng, C. L., Dong, W., Sun, L., Liu, S. Z., Qin, H. F., et al. (2015). Magnetostratigraphy of the Xiaolongtan Formation bearing *Lufengpithecus keiyuanensis* in Yunnan, southwestern China: Constraint on the initiation time of the southern segment of the Xianshuihe-Xiaojiang fault. *Tectonophysics*, *655*, 213–226. https://doi.org/10.1016/j.tecto.2015.06.002

Li, S. H., Deng, C. L., Yao, H. T., Huang, S., Liu, C. Y., He, H. Y., et al. (2013). Magnetostratigraphy of the Dali Basin in Yunnan and implications for late Neogene rotation of the southeast margin of the Tibetan Plateau. *Journal of Geophysical Research: Solid Earth*, *118*, 791–807. https://doi.org/10.1002/jgrb.50129

Li, S. H., Ji, X. P., Harrison, T., Deng, C. L., Wang, S. Q., Wang, L., & Zhu, R. (2020). Uplift of the Hengduan Mountains on the southeastern margin of the Tibetan Plateau in the late Miocene and its paleoenvironmental impact on hominoid diversity. *Palaeogeography, Palaeoclimatology, Palaeoecology*, *553*, 109794. https://doi.org/10.1016/j.palaeo.2020.109794

Li, S. H., van Hinsbergen, D. J., Najman, Y., Liu-Zeng, J., Deng, C. L., & Zhu, R. X. (2020). Does pulsed Tibetan deformation correlate with Indian plate motion changes? *Earth and Planetary Science Letters*, *536*, 116144. https://doi.org/10.1016/j.epsl.2020.116144

Li, S. Y., Currie, B. S., Rowley, D. B., & Ingalls, M. (2015). Cenozoic paleoaltimetry of the SE margin of the Tibetan Plateau: Constraints on the tectonic evolution of the region. *Earth and Planetary Science Letters*, *432*, 415–424.

Linnemann, U., Su, T., Kunzmann, L., Spicer, R. A., Ding, W. N., Spicer, T. E. V., et al. (2018). New U-Pb dates show a Paleogene origin for the modern Asian biodiversity hot spots. *Geology*, *46*(1), 3–6. https://doi.org/10.1130/G39693.1

Liu-Zeng, J., Tapponnier, P., Gaudemer, Y., & Ding, L. (2008). Quantifying landscape differences across the Tibetan Plateau: Implications for topographic relief evolution. *Journal of Geophysical Research*, *113*, F04018. https://doi.org/10.1029/2007JF000897

Liu-Zeng, J., Zhang, J., McPhillips, D., Reiners, P., Wang, W., Pik, R., et al. (2018). Multiple episodes of fast exhumation since Cretaceous in southeast Tibet, revealed by low-temperature thermochronology. *Earth and Planetary Science Letters*, *490*, 62–76. https://doi.org/10.1016/j.epsl.2018.03.011

McFadden, P., & McElhinny, M. (1988). The combined analysis of remagnetization circles and direct observations in palaeomagnetism. *Earth and Planetary Science Letters*, *87*(1-2), 161–172. https://doi.org/10.1016/0012-821X(88)90072-6

Nie, J., Ruetenik, G., Gallagher, K., Hoke, G., Garzione, C. N., Wang, W., et al. (2018). Rapid incision of the Mekong River in the middle Miocene linked to monsoonal precipitation. *Nature Geoscience*, *11*(12), 944–948. https://doi.org/10.1038/s41561-018-0244-z

Ouimet, W., Whipple, K., Royden, L., Reiners, P., Hodges, K., & Pringle, M. (2010). Regional incision of the eastern margin of the Tibetan Plateau. *Lithosphere*, *2*(1), 50–63. https://doi.org/10.1130/L57.1

Renne, P. R., Balco, G., Ludwig, K. R., Mundil, R., & Min, K. (2011). Response to the comment by W.H. Schwarz et al. on "joint determination of 40K decay constants and 40Ar*/40K for the Fish Canyon sanidine standard, and improved accuracy for 40Ar/39Ar geochronology" by P.R. Renne et al. (2010). *Geochimica et Cosmochimica Acta*, *75*(17), 5097–5100. https://doi.org/10.1016/j.gca.2011.06.021

Roger, F., Calassou, S., Lancelot, J., Malavieille, J., Mattauer, M., Xu, Z. Q., et al. (1995). Miocene emplacement and deformation of the Konga-Shan granite (Xianshui-He fault zone, west Sichuan, China) - geodynamic implications. *Earth and Planetary Science Letters*, *130*(1-4), 201–216. https://doi.org/10.1016/0012-821X(94)00252-T

Rowley, D. B., & Garzione, C. N. (2007). Stable isotope-based paleoaltimetry. *Annual Review of Earth and Planetary Sciences*, *35*(1), 463–508. https://doi.org/10.1146/annurev.earth.35.031306.140155

Royden, L., Burchfiel, B. C., King, R. W., Wang, E., Chen, Z. L., Shen, F., & Liu, Y. P. (1997). Surface deformation and lower crustal flow in eastern Tibet. *Science*, *276*(5313), 788–790. https://doi.org/10.1126/science.276.5313.788

Schoenbohm, L., Whipple, K. X., Burchfiel, B. C., & Chen, L. (2004). Geomorphic constraints on surface uplift, exhumation, and plateau growth in the Red River region, Yunnan Province, China. *Geological Society of America Bulletin*, *116*(7), 895–909. https://doi.org/10.1130/B25364.1

Schoenbohm, L. M., Burchfiel, B. C., & Liangzhong, C. (2006). Propagation of surface uplift, lower crustal flow, and Cenozoic tectonics of the southeast margin of the Tibetan Plateau. *Geology*, *34*(10), 813–816. https://doi.org/10.1130/G22679.1

Searle, M., Yeh, M. W., Lin, T. H., & Chung, S. L. (2010). Structural constraints on the timing of left-lateral shear along the Red River shear zone in the Ailao Shan and Diancang Shan Ranges, Yunnan, SW China. *Geosphere*, *6*(4), 316–338. https://doi.org/10.1130/GES00580.1

Shen, X., Tian, Y., Li, D., Qin, S., Vermeesch, P., & Schwanethal, J. (2016). Oligocene-Early Miocene river incision near the first bend of the Yangze River: Insights from apatite (U-Th-Sm)/He thermochronology. *Tectonophysics*, *687*, 223–231. https://doi.org/10.1016/j.tecto.2016.08.006

Spicer, R. A., Su, T., Valdes, P. J., Farnsworth, A., Wu, F.-X., Shi, G., et al. (2020). Why the 'uplift of the Tibetan Plateau' is a myth. *National Science Review*, nwaa091. https://doi.org/10.1093/nsr/nwaa091

Su, T., Jacques, F., Spicer, R., Liu, Y., Huang, Y., Xing, Y., & Zhou, Z. (2013). Post-Pliocene establishment of the present monsoonal climate in SW China: Evidence from the late Pliocene Longmen megaflora. *Climate of the Past*, *9*(2), 1675–1701. https://doi.org/10.5194/cpd-9-1675-2013

Su, T., Spicer, R. A., Li, S.-H., Xu, H., Huang, J., Sherlock, S., et al. (2019). Uplift, climate and biotic changes at the Eocene–Oligocene transition in south-eastern Tibet. *National Science Review*, *6*(3), 495–504. https://doi.org/10.1093/nsr/nwy062

Tang, M., Liu-Zeng, J., Hoke, G. D., Xu, Q., Wang, W., Li, Z., et al. (2017). Paleoelevation reconstruction of the Paleocene-Eocene Gonjo basin, SE-central Tibet. *Tectonophysics*, *712-713*, 170–181. https://doi.org/10.1016/j.tecto.2017.05.018

Tapponnier, P., Lacassin, R., Leloup, P. H., Scharer, U., Zhong, D. L., Wu, H. W., et al. (1990). The Ailao Shan Red River metamorphic belt—Tertiary left-lateral shear between Indochina and South China. *Nature*, *343*(6257), 431–437. https://doi.org/10.1038/343431a0

Tapponnier, P., Peltzer, G., Le Dain, A. Y., Armijo, R., & Cobbold, P. (1982). Propagating extrusion tectonics in Asia: New insights from simple experiments with plasticine. *Geology*, *10*(12), 611–616. https://doi.org/10.1130/0091-7613(1982)10<611:PETIAN>2.0.CO;2

Tian, Y. T., Kohn, B. P., Gleadow, A. J. W., & Hu, S. B. (2014). A thermochronological perspective on the morphotectonic evolution of the southeastern Tibetan Plateau. *Journal of Geophysical Research: Solid Earth*, *119*, 676–698. https://doi.org/10.1002/2013JB010429

Tian, Y. T., Kohn, B. P., Hu, S., & Gleadow, A. J. W. (2015). Synchronous fluvial response to surface uplift in the eastern Tibetan Plateau: Implications for crustal dynamics. *Geophysical Research Letters*, *42*, 29–35. https://doi.org/10.1002/2014GL062383

Tong, Y. B., Yang, Z., Zheng, L. D., Xu, Y. L., Wang, H., Gao, L., & Hu, X. Z. (2013). Internal crustal deformation in the northern part of Shan-Thai Block: New evidence from paleomagnetic results of Cretaceous and Paleogene redbeds. *Tectonophysics*, *608*, 1138–1158. https://doi.org/10.1016/j.tecto.2013.06.031

van Hinsbergen, D. J. J., Lippert, P. C., Li, S., Huang, W., Advokaat, E. L., & Spakman, W. (2019). Reconstructing Greater India: Paleogeographic, kinematic, and geodynamic perspectives. *Tectonophysics*, *760*, 69–94. https://doi.org/10.1016/j.tecto.2018.04.006

Wang, E., Burchfiel, B. C., Royden, L. H., Chen, L. Z., Chen, J. S., Li, W. X., & Chen, Z. L. (1998). Late Cenozoic Xianshuihe-Xiaojiang, Red River, and Dali Fault Systems of Southwestern Sichuan and Central Yunnan, China. *Geological Society of America Special Papers*, *327*, 1–108.

Wang, E., Kirby, E., Furlong, K. P., van Soest, M., Xu, G., Shi, X., et al. (2012). Two-phase growth of high topography in eastern Tibet during the Cenozoic. *Nature Geoscience*, *5*(9), 640–645. https://doi.org/10.1038/ngeo1538

Wang, S. F., Jiang, G. G., Xu, T. D., Tian, Y. T., Zheng, D. W., & Fang, X. M. (2012). The Jinhe-Qinghe fault—An inactive branch of the Xianshuihe-Xiaojiang fault zone, Eastern Tibet. *Tectonophysics*, *544*, 93–102.

Wang, W. M. (1996). A palynological survey of Neogene strata in Xiaolongtan Basin, Yunnan Province of South China. *Acta Botanica Sinica*, *38*, 743–748. (in Chinese with English abstract)

Wang, Y., Zhang, B., Schoenbohm, L. M., Zhang, J., Zhou, R., Hou, J., & Ai, S. (2016). Late Cenozoic tectonic evolution of the Ailao Shan-Red River fault (SE Tibet): Implications for kinematic change during plateau growth. *Tectonics*, *35*, 1969–1988. https://doi.org/10.1002/2016TC004229

Wang, Y., Zhang, P., Schoenbohm, L. M., Zheng, W., Zhang, B., Zhang, J., et al. (2018). Two-phase exhumation along major shear zones in the SE Tibetan Plateau in the Late Cenozoic. *Tectonics*, *37*, 2675–2694. https://doi.org/10.1029/2018TC004979

Wei, H. H., Wang, E., Wu, G.-L., & Meng, K. (2016). No sedimentary records indicating southerly flow of the paleo-Upper Yangtze River from the First Bend in southeastern Tibet. *Gondwana Research*, *32*, 93–104. https://doi.org/10.1016/j.gr.2015.02.006

Wilson, C. J. L., & Fowler, A. P. (2011). Denudational response to surface uplift in east Tibet: Evidence from apatite fission-track thermochronology. *Geological Society of America Bulletin*, *123*(9-10), 1966–1987. https://doi.org/10.1130/B30331.1

Wissink, G. K., Hoke, G. D., Garzione, C. N., & Liu-Zeng, J. (2016). Temporal and spatial patterns of sediment routing across the southeast margin of the Tibetan Plateau: Insights from detrital zircon. *Tectonics*, *35*, 2538–2563. https://doi.org/10.1002/2016TC004252

Wu, J., Zhang, K., Xu, Y., Wang, G., Garzione, C. N., Leloup, P. H., Sorrel, P., & Mahéo, G. (2018). Paleoelevations in the Jianchuan Basin of the southeastern Tibetan Plateau based on stable isotope and pollen grain analyses. *Palaeogeography, Palaeoclimatology, Palaeoecology*, *53*, 93–108. https://doi.org/10.1016/j.palaeo.2018.03.030

Xiong, J., Li, Y., Zhong, Y., Si, S., & Yao, Y. (2016). Paleomagnetism of the Jianshui basin in Yunnan, SW China, and geomorphological evolution of the Yunnan Plateau since the Neogene. *Journal of Asian Earth Sciences*, *123*, 67–77. https://doi.org/10.1016/j.jseaes.2016.04.005

Xu, G., & Kamp, P. J. J. (2000). Tectonics and denudation adjacent to the Xianshuihe Fault, eastern Tibetan Plateau: Constraints from fission track thermochronology. *Journal of Geophysical Research*, *105*(B8), 19,231–19,251. https://doi.org/10.1029/2000JB900159

Xu, J., Ferguson, D. K., Li, C. S., & Wang, Y. F. (2008). Late Miocene vegetation and climate of the Luhe region in Yunnan, southwestern China. *Review of Palaeobotany and Palynology*, *148*(1), 36–59. https://doi.org/10.1016/j.revpalbo.2007.08.004

Yan, Y., Carter, A., Huang, C.-Y., Chan, L.-S., Hu, X.-Q., & Lan, Q. (2012). Constraints on Cenozoic regional drainage evolution of SW China from the provenance of the Jianchuan Basin. *Geochemistry, Geophysics, Geosystems*, *13*, Q03001. https://doi.org/10.1029/2011GC003803

Yang, R., Willett, S. D., & Goren, L. (2015). In situ low-relief landscape formation as a result of river network disruption. *Nature*, *520*(7548), 526–529. https://doi.org/10.1038/nature14354

Yang, Z., Shen, C., Ratschbacher, L., Enkelmann, E., Jonckheere, R., Wauschkuhn, B., & Dong, Y. (2017). Sichuan Basin and beyond: Eastward foreland growth of the Tibetan Plateau from an integration of Late Cretaceous-Cenozoic fission-track and (U-Th)/He ages of the eastern Tibet Plateau, Qinling, and Daba Shan. *Journal of Geophysical Research: Solid Earth*, *122*, 4712–4740. https://doi.org/10.1002/2016JB013751

Yunnan Bureau of Geology and Mineral Resource (YBGMR), 1990. Regional geology of Yunnan Province, pp. 1–726 (In Chinese).

Zhang, H., Oskin, M. E., Liu-Zeng, J., Zhang, P., Reiners, P. W., & Xiao, P. (2016). Pulsed exhumation of interior eastern Tibet: Implications for relief generation mechanisms and the origin of high-elevation planation surfaces. *Earth and Planetary Science Letters*, *449*, 176–185. https://doi.org/10.1016/j.epsl.2016.05.048

Zhang, P., Najman, Y., Mei, L., Millar, I., Sobel, E., Carter, A., et al. (2019). Palaeodrainage evolution of the large rivers of East Asia, and Himalayan-Tibet tectonics. *Earth-Science Reviews*, *192*, 601–630. https://doi.org/10.1016/j.earscirev.2019.02.003

Zhang, Y. Z., Replumaz, A., Leloup, P. H., Wang, G. C., Bernet, M., Van Der Beek, P., et al. (2017). Cooling history of the Gongga batholith: Implications for the Xianshuihe Fault and Miocene kinematics of SE Tibet. *Earth and Planetary Science Letters*, *465*, 1–15. https://doi.org/10.1016/j.epsl.2017.02.025

Zhu, R. X., Liu, Q. S., Yao, H. T., Guo, Z. T., Deng, C. L., Pan, Y. X., et al. (2005). Magnetostratigraphic dating of hominoid-bearing sediments at Zhupeng, Yuanmou Basin, southwestern China. *Earth and Planetary Science Letters*, *236*(3-4), 559–568. https://doi.org/10.1016/j.epsl.2005.05.039

Zhu, R. X., Potts, R., Pan, Y. X., Lü, L. Q., Yao, H. T., Deng, C. L., & Qin, H. F. (2008). Paleomagnetism of the Yuanmou Basin near the southeastern margin of the Tibetan Plateau and its constraints on late Neogene sedimentation and tectonic rotation. *Earth and Planetary Science Letters*, *272*(1-2), 97–104. https://doi.org/10.1016/j.epsl.2008.04.016